Journal of Molecular Catalysis A: Chemical 293 (2008) 1–7

Contents lists available at ScienceDirect

Journal of Molecular Catalysis A: Chemical

journal homepage: www.elsevier.com/locate/molcata

Editors' Choice Paper

Catalytic autoxidations using tris-diimine iron(II) coordination complexes

Ana Ison, Cheng Xu [1], G. Ken Weakley, David E. Richardson *

Center for Catalysis, Department of Chemistry, University of Florida, Gainesville, FL 32611-7200, United States

ARTICLE INFO

Article history:
Received 21 December 2007
Received in revised form 17 June 2008
Accepted 18 June 2008
Available online 27 June 2008

Keywords:
Autoxidation
Cumene
Cyclohexane
Oxidation
Radicals
Adipic acid
Peroxides

ABSTRACT

The hydrocarbon-soluble coordination complex [Fe(4,7-diphenyl-1,10-phenanthroline)$_3$](SO$_3$CF$_3$)$_2$ (**1**) is an active catalyst for the autoxidation of cumene and cyclohexane. The activity of **1** in the autoxidation of cumene at 60 °C is comparable to that of tetra(pentafluorophenyl)porphyrin iron(III) chloride (**2**), a halogenated iron porphyrin with high autoxidation activity. The kinetic data have been fit by a mechanism in which the iron catalyst is activated by reaction with peroxide and the resulting active complex acts as a peroxide decomposition catalyst producing chain-carrying radicals. The activity of **1** is also comparable to that of **2** in the autoxidation of cyclohexane at 135 °C. The utility of catalyst **1** is enhanced by its solubility in pure hydrocarbon substrates.

1. Introduction

We have investigated the mechanism of catalysis of hydrocarbon autoxidation by an iron(II) tris-diimine coordination complex, [Fe(DPP)$_3$](SO$_3$CF$_3$)$_2$ (DPP = 4,7-diphenyl-1,10-phenanthroline, **1**), which has catalytic activity [1,2] comparable to that of halogenated iron porphyrins [3–7]. A radical mechanism has been proposed for the porphyrin catalysts in which catalytic decomposition of alkyl hydroperoxides [3–13] generates chain-propagating radicals ROO• and RO•. This mechanism for halogenated iron porphyrin catalysts is supported by the experimental observation that the rate of substrate oxidation increases with the catalyst efficiency in disproportionation of the corresponding alkyl hydroperoxide [7], and the mechanism and rate constants proposed by Labinger and co-workers [10–13] closely model the experimental results of Lyons and co-workers [3–7]. The porphyrin catalysts therefore operate via the classic radical chain mechanism that has been well documented in the literature [14–18].

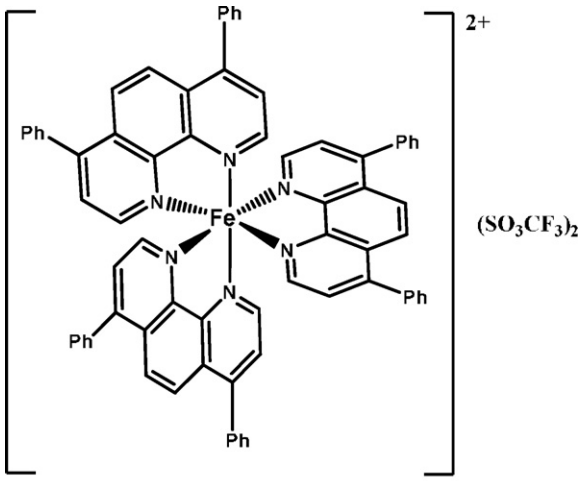

1

Cumene was chosen as the substrate for kinetic studies because of its high boiling point, its reactive tertiary C–H bond, the extensive literature on its autoxidation, and the stability of cumyl hydroperoxide. To provide direct comparisons to halogenated porphyrin catalysts [3–7,10–13,19], tetra-(pentafluorophenyl)-porphyrin iron(III) chloride (**2**) was used in parallel experiments. In addition, the catalytic autoxidation of cyclohexane was investigated to demonstrate application of **1** in secondary C–H oxidations.

* Corresponding author. Tel.: +1 352 392 6736; fax: +1 352 392 3255.
E-mail address: der@chem.ufl.edu (D.E. Richardson).

[1] The authors dedicate this article to the late Cheng Xu, Ph.D., an outstanding scientist and friend. He was the first to observe the unusual reactivity of the catalyst described in this work for hydrocarbon autoxidation.

1381-1169/$ – see front matter © 2008 Elsevier B.V. All rights reserved.
doi:10.1016/j.molcata.2008.06.010

2. Experimental

2.1. General

Product analysis was done using the following instruments: Varian CP-3800 GC/FID with a DB-35MS column, Varian 300 Mz NMR, Finnigan MAT95 Q GC/MS. Oxidation and peroxide decomposition reactions were done in a glass-lined stainless steel Parr 4560 300 mL Mini Bench Top Reactor. The reactor was modified to allow headspace and liquid sampling during reactions. Constant O_2 pressure was maintained by using a gas burette. O_2 gas uptake (oxidation) or production (peroxide decomposition) was monitored by a pressure transducer connected to a Cole-Parmer Solid State Paperless Data Recorder.

2.2. Materials

Cumene and benzene of the highest purity were purchased from Aldrich, distilled over Na and stored under an inert atmosphere. Cyclohexane was distilled over CaH_2. Fe(III)-tetra-(pentafluorophenyl)-porphyrin chloride (FeTPPF) was purchased from Mid-Century and used as received. $Fe(SO_3CF_3)_2{\cdot}6H_2O$, Fe(4,7-diphenylphenanthroline)$_3Cl_2$ and Ru(4,7-diphenyl-1,10-phenanthroline)$_3Cl_2$ were synthesized using published procedures [20,21]. All other materials were purchased from Aldrich and used without further purification.

2.3. Oxidation kinetics

Cumene oxidation was done by charging the reactor with a specified amount of catalyst and cumene, cumene/benzene or cumene/*o*-dichlorobenzene. The reactor was pressurized to 50 psi O_2 and heated to 60 °C. Once the temperature was reached a constant O_2 feed was maintained at 60 psi during the entire reaction time. The reaction solution was sampled periodically during the oxidation and analyzed by GC/FID (ROH, R′=O, ROOH) and ^{1}H NMR (ROOR). All products were characterized by GC/MS. Cyclohexane oxidation was done by charging the reactor with a specified amount of catalyst and cyclohexane/*o*-dichlorobenzene solution. The reactor was pressurized to 60 psi and heated to 135 °C. Once heated, a constant O_2 feed was maintained at 80 psi. The reaction solution was sampled periodically and analyzed by GC/FID.

2.4. Peroxide decomposition kinetics

The reactor was charged with 95 mL benzene under an inert atmosphere. The reactor was heated to 60 °C and 5 mL ROOH was added by syringe, immediately followed by the addition of 5 mL of a benzene solution of the catalyst. The reaction solution was sampled periodically and analyzed by GC/FID. Oxygen release was monitored by a pressure transducer.

2.5. Synthesis of [Fe(4,7-diphenyl-1,10-phenanthroline)$_3$] $(SO_3CF_3)_2{\cdot}H_2O$

Ten milliliters of a 1 M $AgCF_3SO_3$ aqueous solution was added to 10 mL of a 0.5 M $FeCl_2$ aqueous solution. A white precipitate (AgCl) formed immediately upon mixing. The solution was allowed to stir for 3 h before filtering. The filtrate containing an aqueous solution of $Fe(CF_3SO_3)_2$ was added to 30 mL of an ethanolic solution of 0.5 M DPP. The solution immediately turned dark red. The dark red solution was allowed to stir for 3 h uncovered allowing the solution volume to reduce to ~10 mL. The resulting solution contained a dark red precipitate, which was isolated and washed with small amounts of ethanol. Dark red solid was dried in a vacuum oven at 65 °C for 6 h resulting in dark red powder (yield 87%). ^{1}H NMR (300 MHz, DMSO): δ8.3 (6H, s, phen H5,6), δ8.0 (6H, d, J = 5.7, phen H2,9), δ7.8 (6H, d, J = 5.7, phen H3,8), δ7.7–7.6 (30H, m, phenyl groups). ^{13}C NMR (75 MHz $CDCl_3$): δ156.5, δ150.0, δ149.4, δ135.3, δ129.9, δ129.7, δ129.1, δ128.1, δ127.0, δ125.9. Anal. Calcd. for; $Fe_1C_{74}H_{50}N_6O_7F_6S_2$ (%): C, 64.91; H, 3.68; N, 6.14. Found (%): C, 64.72; H, 3.51; N, 6.07. Electron spray ionization spectroscopy (ESI-MS): MW = 1053 [$Fe(DPP)_3^{2+}$]; MW = 869 [$Fe(DPP)_2(SO_3CF_3)^+$]; MW = 720 [$Fe(DPP)_2^{2+}$]; MW = 333 [$HDPP^+$].

2.6. Kinetic modeling

Numerical kinetic simulations were done with Kinetica99, a program based on the Gear integration method (D.E. Richardson, University of Florida, 1999). The concentration vs. time profiles calculated by this program are identical to those calculated by other numerical integration programs for chemical kinetics.

3. Results and discussion

3.1. Cumene autoxidation

3.1.1. Conversions and selectivities

Oxidation reactions were carried out in a glass lined, Teflon capped stainless steel pressure reactor with liquid sampling at regular intervals during the reactions. Catalyst concentrations (usually 57 μM) were below the solubility limits of the reaction mixture. The products were analyzed by GC/FID, GC/MS or ^{1}H NMR. The major products of catalyzed cumene oxidation and cumyl peroxide decomposition are cumyl alcohol (ROH), acetophenone (R′=O), cumyl hydroperoxide (ROOH) and small amounts of dicumylperoxide (ROOR), as shown below.

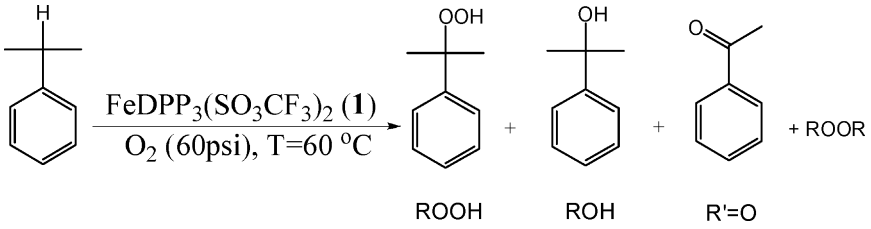

Product conversions reported in Table 1 show **1** and **2** are similar in catalytic activity for cumene oxidation by O_2 but show differences in the cumyl hydroperoxide and acetophenone selectivities. Oxygen uptake stoichiometry exceeds the oxidized products reported in Table 1 as a result of side reactions leading to other undetected oxidation products such as formaldehyde, CO, and CO_2. For the reactions described in Table 1, 74 ± 2% and 69 ± 5% of the oxygen consumed are in the observed products for catalyst **1** and **2**, respectively. Both CO and CO_2, products of formaldehyde oxidation,

Table 1
Autoxidation of cumene catalyzed by **1** and **2**[a]

	Catalyst		Uncatalyzed[b]
	1	**2**	
% conversion	15.1 ± 1.2	15.8 ± 1.8	Trace
% ROOH	14.8 ± 1.5	4.6 ± 0.4	Trace
% ROH	73.1 ± 0.6	78.2 ± 1.4	nd
% R′=O	11.9 ± 0.9	17.2 ± 1.3	nd
% ROOR	~2	~2	nd
O_2 uptake (mol)	0.042 ± 0.001	0.047 ± 0.005	Trace

[a] Reactions done at 60 °C and 60 psi of constant O_2 pressure; catalyst = 57 μM; 50 mL cumene; 50 mL benzene; reaction time = 5 h; Results and errors calculated from at least five experiments for each catalyst. nd = not detected.

[b] Numerical fits of Scheme 1 in the absence of steps 9–13 are in agreement with the uncatalyzed reaction results. Product abbreviations: cumyl alcohol (ROH), acetophenone (R′=O), cumyl hydroperoxide (ROOH), dicumylperoxide (ROOR).

were detected in the headspace by GC but were not quantified, so oxygen is also consumed in the overoxidation of the substrate via formaldehyde formation.

Both catalytic reactions have substantial induction periods. The induction periods are ~35 min for **1** and ~70 min for **2**-catalyzed oxidation reactions under our conditions (Figs. 1 and 2). Typically induction periods are highly dependent on substrate purity and other factors [14]. The induction periods disappear with addition

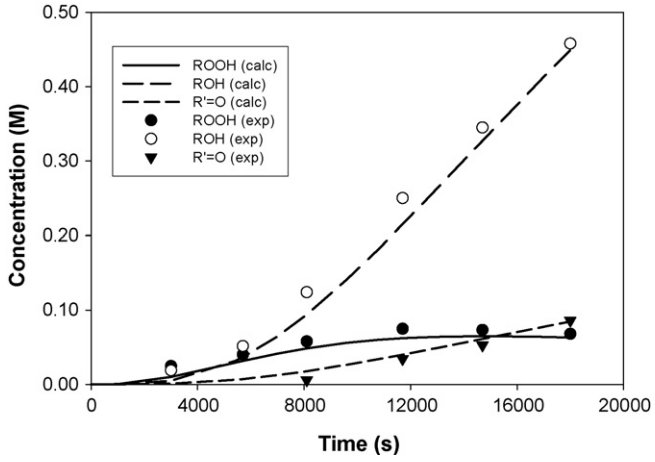

Fig. 1. Cumene autoxidation data and model results for catalyst **1**.

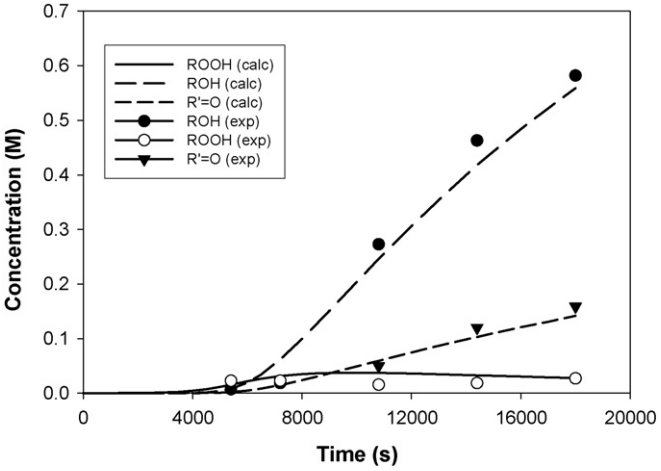

Fig. 2. Cumene autoxidation data and model results for catalyst 2.

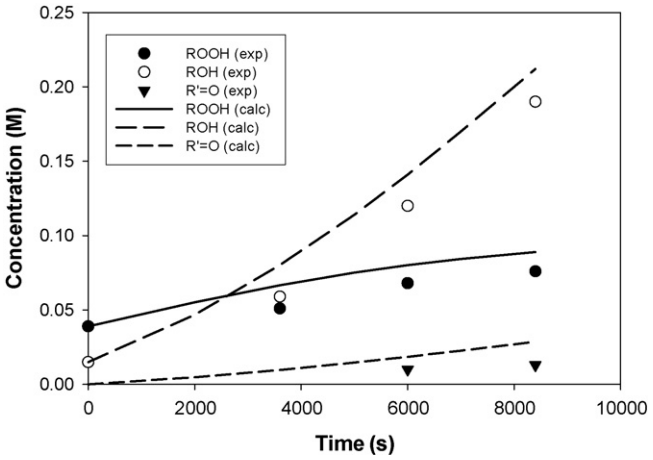

Fig. 3. Cumene autoxidation data and model results for catalyst **1** with added ROOH (0.04 M). The induction period in Fig. 1 is not observed when peroxide is added.

of small amounts (0.04 M) of cumyl hydroperoxide (Figs. 3 and 4). Water (0.5 M) also decreases the induction period in the case of **2** only, as previously described in the literature [19].

In addition to comparisons with **2**, we also did parallel experiments using the widely employed Co naphthanate in the same concentration. Only trace amounts of products were detected at the standard 60 °C reaction temperature, and the reactivity was essentially the same as the uncatalyzed case. Increasing the reaction temperature to 100 °C did increase the overall conversion to 10%.

3.1.2. Oxygen dependence

The oxygen pressure dependence in cumene oxidation catalyzed by **1** was investigated over a pressure range of 30–100 psi. Oxygen uptake rates and product distributions are essentially unaffected within experimental error (±10%) by a change in pressure, indicating a zero-order dependence on O_2.

3.1.3. Temperature dependence

The observed effect of increasing the reaction temperature in autoxidation reaction with **1** is increased selectivity toward the secondary oxidation products, ROH, R′=O, etc. The ROOH concentration increases to a maximum at 80 °C, then decreases at

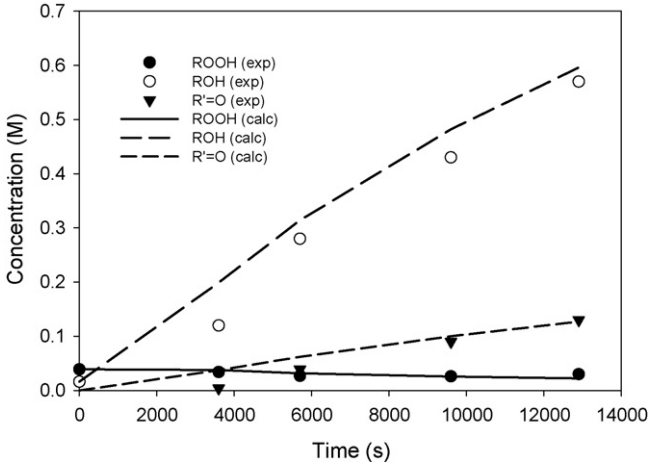

Fig. 4. Cumene autoxidation data and model results for catalyst **2** with added ROOH (0.04 M). The induction period in Fig. 2 is not observed when peroxide is added.

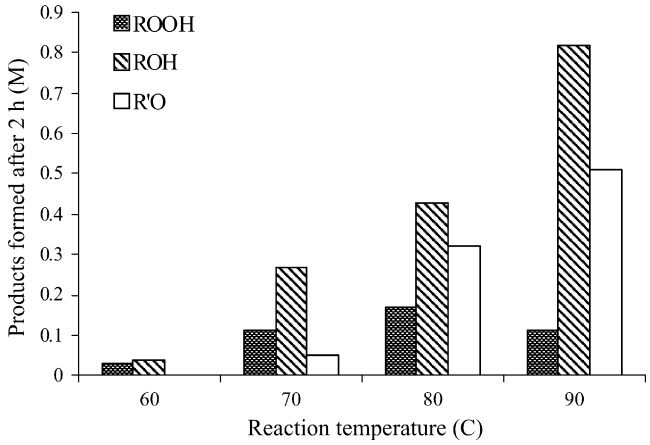

Fig. 5. Temperature effects on product selectivity for cumene oxidation catalyzed by **1**.

higher temperatures. The conversion to ROH and R′=O increases as expected for an autoxidation mechanism (Fig. 5).

3.1.4. Metal concentration dependence

The concentration dependence for catalyst **1** was determined in cumene autoxidation experiments and is shown in Fig. 6. Saturation in the rate of oxygen uptake is observed as the catalyst concentration approaches ~600 μM. This kinetic saturation is not the result of solubility limits and can be explained readily by the autoxidation mechanism described below, where the reaction rate is approaching the maximum rate possible for cumene autoxidation with a catalyzed peroxide decomposition. We did not determine the order in **[1]** at pre-saturation concentrations <50 μM.

3.2. Cumyl hydroperoxide decomposition reactions

Both **1** and **2** are potent peroxide decomposition catalysts (Figs. 7 and 8). Induction periods are not observed for the decomposition reactions due to the immediate activation of the catalytic cycle by cumyl hydroperoxide. Experimental k_{obs} values for catalytic cumyl peroxide decomposition by **1** and **2** (both 57 μM) are $4.7 \pm 0.1 \times 10^{-4}\ s^{-1}$ and $1.5 \pm 0.3 \times 10^{-3}\ s^{-1}$, respectively, based on peroxide consumption. As expected, oxygen was formed in approximately half the amount of the ROH produced.

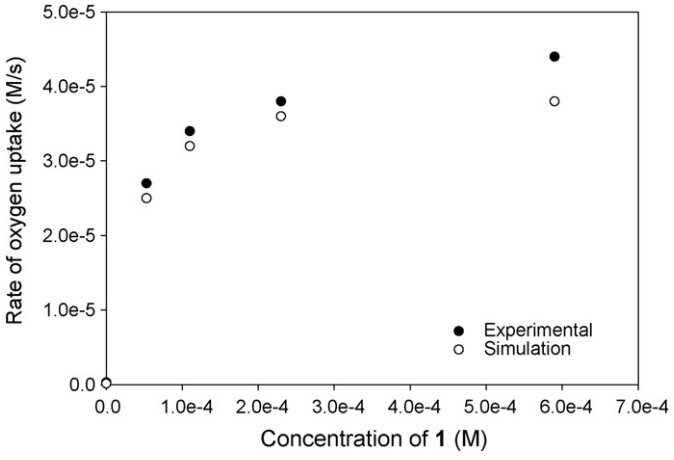

Fig. 6. Experimental and calculated dependence of catalyst concentration on rate of oxygen uptake; 60 °C, 60 psi O_2, 50/50 benzene/cumene, run time = 5 h.

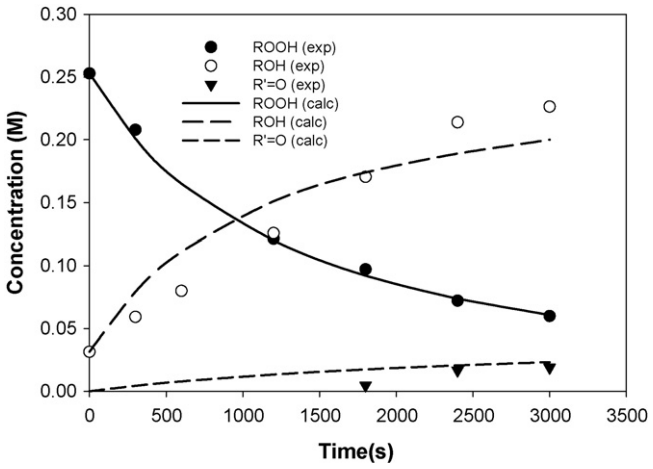

Fig. 7. Peroxide decomposition catalyzed by **1**: data (markers) and model (lines).

3.3. Mechanism

3.3.1. Radical chain model

We propose that **1** has the same role in catalytic hydrocarbon autoxidation as halogenated iron porphyrins. The mechanism proposed by Labinger and co-workers [10,11] for the oxidation of alkanes catalyzed by halogenated iron porphyrins is shown in Scheme 1. Rate constants appropriate for cumene autoxidation at 60 °C are shown in steps 1–8, which describe the well-established mechanism [8,22,23] of background autoxidation occurring in the absence of catalyst. The primary function of the catalyst is to decompose the intermediate alkyl hydroperoxide (ROOH) and generate chain-propagating radicals via steps 9 and 10, where one of the steps is typically fast and the other is rate determining [16]. The weakly oxidizing catalyst **2** (or its activated form) is slowly reduced by the hydroperoxide in step 9, while the active metal catalyst derived from **1** is slowly oxidized by the hydroperoxide and step 10 is rate determining. The rate constants for peroxide decomposition by the active catalytic complexes derived from **1** ($k_{10} = 1.7\ M^{-1}\ s^{-1}$) and **2** ($k_9 = 7.0\ M^{-1}\ s^{-1}$) were estimated by fitting cumyl hydroperoxide decomposition data to the proposed mechanism in Scheme 1 (in both models, the other rate constant was set to the estimated diffusion limit of $10^{10}\ M^{-1}\ s^{-1}$). UV–vis spectra of the catalysts in situ confirm that Fe(II) and Fe(III) species are the resting states for **1** and **2**, respectively. Rate constants for steps 1–4 were based on literature values at 60 ± 5 °C [22–25] while the others were determined

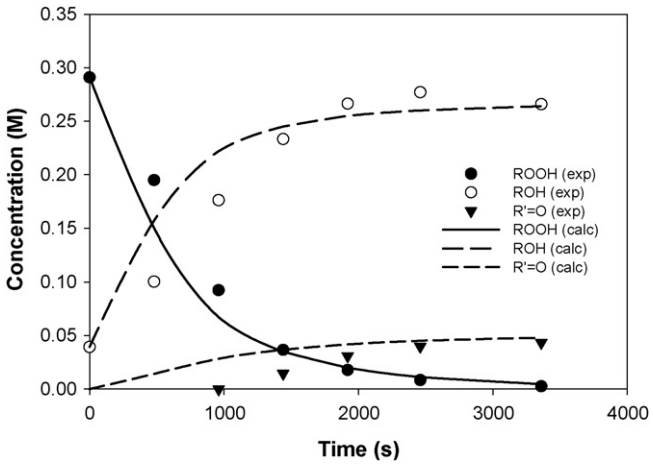

Fig. 8. Peroxide decomposition catalyzed by **2**: data (markers) and model (lines).

Initiation

(1) RH $\xrightarrow{k_1 = 1\times10^{-10}\ s^{-1}}$ R• $\xrightarrow{O_2,\ fast}$ ROO•

Propagation

(2) ROO• + RH $\xrightarrow{k_2 = 1.0\ M^{-1}s^{-1}}$ ROOH + R• $\xrightarrow{O_2,\ fast}$ ROO•

Radical chain and termination steps

(3) 2 ROO• $\xrightarrow{k_3 = 2.4\times10^{5}\ M^{-1}s^{-1}}$ 2 RO• + O_2

(4) 2 ROO• $\xrightarrow{k_4 = 2.2\times10^{4}\ M^{-1}s^{-1}}$ ROOR + O_2

(5) RO• + RH $\xrightarrow{k_5 = 9.6\times10^{4}\ M^{-1}s^{-1}}$ ROH + R• $\xrightarrow{O_2,\ fast}$ ROO•

(6) RO• + ROOH $\xrightarrow{k_6 = 1.2\times10^{6}\ M^{-1}s^{-1}}$ ROH + ROO•

(7) RO• $\xrightarrow{k_7 = 8.4\times10^{4}\ s^{-1}}$ R'=O + Me• $\xrightarrow{O_2,\ fast}$ MeOO•

(8) MeOO• + ROO• $\xrightarrow{fast}$ ROH + CH_2O + O_2

Catalytic Steps

(9) ROOH + M^{III} $\xrightarrow{k_9}$ ROO• + H^+ + M^{II}

(10) ROOH + M^{II} $\xrightarrow{k_{10}}$ RO• + HO^- + M^{III}

Scheme 1. Catalytic radical chain mechanism for hydrocarbon autoxidation. In this mechanism, metal catalysts produce chain carriers ROO and R′=O via the decomposition of the ROOH. Rate constants in steps 1–8 model the autoxidation of cumene in the absence of added catalyst.

from kinetic fits of several experimental data sets for autoxidation and peroxide disproportionation. Initial values for unknown rate constants were obtained by analogy to known rate constants for similar substrates.

Oxidation in the absence of added peroxide relies on the slow initiation of the autoxidation chain due to the presence of adventitious activators. The origins of the variability of induction periods are notoriously difficult to determine [14]. The differences in induction periods for **1** and **2** are not readily explained, but they may be associated with different catalyst activation chemistry for the two classes of catalysts. In view of the short induction period compared to catalyst **2**, catalyst **1** appears to either more rapidly initiate the autoxidation (via some specific initiation step, impurities in the catalyst, or another mechanism) or it may be activated more rapidly by peroxide or some other product produced in the autoxidation. These possibilities can be handled in simulations through either adjustment of the initiation rate constant in Scheme 1 or, e.g., addition of steps in which catalyst **1** is activated by peroxide. We chose the latter approach, and fits (Figs. 1 and 2) to the experimental induction periods could be obtained if an additional step is included in which prior to catalyzed ROOH decomposition each complex must be converted to an active form of the catalyst [19,26] (steps 11–13 in Scheme 2) by reaction with ROOH (or H_2O in the case of **2**) produced initially by the slow uncatalyzed autoxidation reaction (Table 2). These steps were therefore included in our simulations since we wanted to provide a kinetic model for the variations in both the induction periods and the steady state autoxidation rates

(11) $FeDPP_3$ (**1**) + ROOH $\xrightarrow{k_{11}=10\ M^{-1}s^{-1}}$ **1'** (active catalyst)

(12) FeTPPF (**2**) + ROOH $\xrightarrow{k_{12}=0.04\ M^{-1}s^{-1}}$ **2'** (active catalyst)

(13) FeTPPF (**2**) + H_2O $\xrightarrow{k_{13}=0.004\ M^{-1}s^{-1}}$ **2''** (active catalyst)

Scheme 2. Activation of **1** and **2** by reaction with ROOH (or water in the case of 13). Rate constants are those required to fit the observed induction periods (Figs. 1 and 2).

Table 2
Experimental and model results for ROOH and H_2O effects[a]

	% conversion	% ROOH	% ROH	% R′=O
1 + ROOH[b]	8	27	68	5
Calculated	9	27	64	9
2 + ROOH[c]	20	4	78	18
Calculated	21	3	80	17
2 + H_2O[d]	25	4	72	24
Calculated	23	3	81	17

[a] Cumyl hydroperoxide or water was added to cumene/benzene initially to observe the effect on induction period. Induction period was not present in any of the above experiments. Calculated values are from the model given in Schemes 1 and 2 in the text.

[b] [ROOH] = 4×10^{-2} M, reaction time = 2.3 h.

[c] [ROOH] = 4×10^{-2} M, reaction time = 3.5 h.

[d] [H_2O] = 0.5 M, reaction time = 5 h.

(we emphasize that there are many other possible explanations for the variation in induction periods).

In this scheme, the formation of the active catalyst from precursor **1** occurs more rapidly resulting in a shorter induction period than that for **2**. Although the rate for the activation of **1** (step 11) is faster than that for **2**, the latter still proves to be a superior peroxide decomposition catalyst once activated. We note that catalyst activation with ligand dissociation or displacement is almost certainly required for $FeDPP_3$ since the Ru analog has no activity and addition of DPP retards the catalysis for **1** (see ligand addition experiments below). Addition of cumyl peroxide essentially eliminates the induction period observed in the reactions with cumene and catalyst both experimentally and in simulations based on Scheme 1. The initiation by addition of peroxide is well known in autoxidation chemistry [8].

The stability of the intermediate cumyl hydroperoxide is a significant advantage of cumene as a substrate since its catalyzed decomposition can be studied independently in the presence of the autoxidation catalysts. Thus, rate constants for the crucial peroxide decomposition steps in the autoxidation mechanism of Scheme 1 can be determined in separate experiments, providing a classic test of the metal-catalyzed peroxide decomposition autoxidation mechanism [15,16,18]. Schemes 1 and 2 provide a reasonable model that fits all of the experimental data, including induction periods. Schemes 1 and 2 show the rate constants obtained by simultaneous numerical fitting of cumene oxidation and cumyl hydroperoxide decomposition data for **1** to the mechanism (Figs. 1, 3 and 7).

The global fit does show some deviation from the experimental data, especially in the peroxide decomposition experiments where the fits predict a rate of ROH production that is somewhat higher than experimentally observed (Figs. 7 and 8) (note that the apparently sigmoidal appearance of the ROH curves results from the presence of the fit curve in the plot; the ROH appearance data do not have significant sigmoidal character when plotted alone). The model rate constants predict pseudo-first order k_{obs} values close to those of the experiments based on ROOH disappearance. Table 3 gives the experimental and calculated k_{obs} values using the model, showing that both the decomposition rates are simulated accurately by the same rate constants that fit the autoxidation data. This provides strong evidence that, as for **2**, catalyst **1** functions as a peroxide decomposition catalyst rather than forming high-valent iron intermediates that react directly with the substrate. As with the iron porphyrins [27] and other purported oxygenase mimics (e.g., see recent a recent analysis by Yin and Finke [28]), a high-valent iron intermediate is not required to explain the experimental observations.

The dependence of autoxidation reactions on oxygen pressure is expected to be zero, even at atmospheric pressure. Considering

Table 3
Experimental and calculated k_{obs} values for catalyzed peroxide decomposition

	1	2	$RuDPP_3Cl_2$
k_{obs} (exp) ($M^{-1}\,s^{-1}$)[a]	$4.7 \pm 0.1 \times 10^{-4}$	$1.5 \pm 0.3 \times 10^{-3}$	No decomposition
k_{obs} (calc) ($M^{-1}\,s^{-1}$)[b]	5.0×10^{-4}	1.2×10^{-3}	–

Reactions done in a Parr reactor at 60 °C under argon; catalyst = 5.7×10^{-6} mol; ROOH = 5 mL; benzene 95 mL; reaction time ≅1 h; No decomposition over 4 h in the absence of catalyst.

[a] k_{obs} (exp) values obtained from first-order fits of experimental data for the disappearance of ROOH.

[b] k_{obs} (calc) values obtained from first-order fits of the model calculated values for ROOH disappearance.

the mechanism in Scheme 1, the diffusion-controlled addition of molecular oxygen to R• is the only step where oxygen is a reactant.

The maximum rate of oxidation is an important parameter for metal-catalyzed autoxidation reactions [16,29,30]. The maximum theoretical rate of oxidation is dependent on the substrate and is determined by the propagation and termination rate constants. The maximum rate equation derived [30] from the general autoxidation mechanism is shown in Eq. (1),

$$-\frac{d[RH]}{dt} = \frac{k_p^2[RH]^2}{2k_t} \quad (1)$$

where k_p and k_t are the propagation and termination rate constants, respectively [29]. Eq. (1) holds true in the presence of metal catalysts as long as they do not catalyze the propagation and termination steps (note that the more general equation derived by Walling [30] depends on the details of the initiation chemistry and reaction stoichiometry; here we use a simple form often applied when such details are not known). The rate of oxygen uptake for metal-catalyzed autoxidation can be increased only up to a limiting value by addition of catalyst. The theoretical limiting rate for cumene at 60 °C calculated from Eq. (1) is 3.1×10^{-5} M s^{-1} and was obtained using $k_p = 1.0\,M^{-1}\,s^{-1}$ and $k_t = 2.1 \times 10^5\,M^{-1}\,s^{-1}$, which were estimated from literature activation energy values appropriate for 60 °C [31,32].

The maximum rate was also calculated through simulations using our proposed mechanism and rate constants shown in Scheme 1, yielding a value of 3.8×10^{-5} M s^{-1}. The maximum rate was also determined experimentally by increasing the concentration of **1** until the rate of oxygen uptake leveled off. The experimental maximum rate is 4.4×10^{-5} M s^{-1} (Fig. 6). The general agreement of the estimated maximum rate, current model prediction, and experimental values shows that the active role of the catalyst is confined primarily to the decomposition of peroxide and therefore is consistent with a radical autoxidation mechanism as shown in Scheme 1. The reaction order in catalyst was not determined in this work, but could in principle be studied using much lower concentrations than those used here. The rate saturation with increasing catalyst concentration (Fig. 6) is, however, completely consistent with a mechanism in which the sole role of the catalyst is to decompose peroxide.

3.3.2. Role of ligand dissociation

The possible involvement of ligand dissociation in activation of **1** was investigated. Complex **1** is formed in situ (UV–vis) when $Fe(SO_3CF_3)_2$ plus 1, 2, 3, or 6 equiv. of DPP are used to catalyze the reaction. Product conversions increase from 1 to 3 equiv. along with a parallel increase in the concentration of **1** (Table 4). Using 6 equiv. of DPP results in a large decrease in conversion although the in situ concentration of **1** is high. Adding 3 equiv. of DPP to a **1**-catalyzed oxidation also leads to inhibition. Addition of 3 equiv. DPP to catalyst **2** has no effect on conversion (Table 4), so DPP itself is not a general autoxidation inhibitor. These results suggest that ligand dissociation is an important step in the activation of **1** since equilibrium DPP dissociation would be suppressed by the presence of free ligand.

Table 4
Ligand and counterion effects[a]

	Equiv. DPP[b]	% conversion
Catalyst		
1[c]	0	15
	3	2
1[d]	0	12
2[c]	0	19
	3	23
Complex		
$Fe(Trf)_2$[c]	1	4
	2	8
	3	10
	6	2
$RuDPP_3Cl_2$[d]	0	Trace
$FeDPP_3Cl_2$[d]	0	10

[a] Reaction conditions same as in Table 1 footnote unless specified.

[b] Number of equivalents based on moles of metal complex (57 μM). Trf = $(SO_3CF_3)^-$.

[c] 100 mL cumene.

[d] 50 mL/50 mL cumene/*o*-dichlorobenzene.

The role of the counterion in the activation of catalyst was investigated by comparing **1** to $FeDPP_3Cl_2$. Due to low solubility of the chloride salt in benzene/cumene, *o*-dichlorobenzene was used as co-solvent in which case both FeDPP chloride and triflate salts have comparable activities (Table 4). The ruthenium(II) analogue of **1** ($RuDPP_3Cl_2$), although soluble, has no catalytic activity in either autoxidation or peroxide decomposition (Table 4), presumably because of its lower tendency to dissociate due to inert Ru–N bonds.

3.3.3. Catalyst lifetime

Active catalyst lifetime can be assessed by comparing the experimental oxygen uptake curve over a long reaction time to the oxygen uptake curve predicted by the proposed mechanistic scheme (Fig. 9).

The proposed mechanism does not include any steps leading to catalyst destruction; therefore, the predicted oxygen uptake curve does not take into consideration any decrease in the rate due to

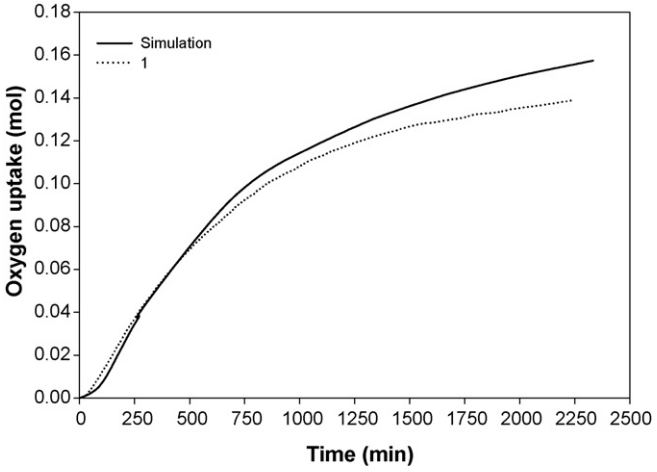

Fig. 9. Comparison of oxygen uptake curve during cumene oxidation catalyzed by **1** and a curve predicted by simulation using proposed mechanism for a reaction time up to 37 h.

catalyst degradation. Comparison of the predicted oxygen uptake curve to that of the experimental curve shows that experimentally oxygen uptake levels off earlier than predicted suggesting some catalyst degradation is occurring, perhaps by coordination with the more polar oxidation products. The difference becomes significant only at reaction times well beyond the 5-h reaction time of the standard runs used in our experiments. The results indicate the active catalyst is robust and remains active for an extended period of time during the reaction.

3.4. Cyclohexane autoxidation

Complex **1** was also investigated in the autoxidation of cyclohexane (Table 5). The conversion was 8% in 2 h to form cyclohexanol (41%), cyclohexanone (47%), and adipic acid (12%) under similar conditions (except $T = 135\,^{\circ}C$) [2].

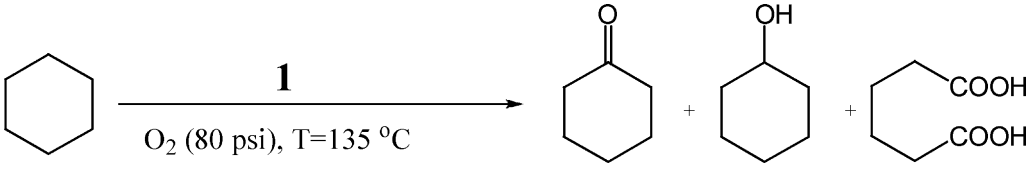

Although soluble, $RuDPP_3Cl_2$ was inactive for cyclohexane oxidation, as found for cumene autoxidation. Oxidation catalyzed by **2** yields a 5% conversion with cyclohexanol, cyclohexanone, and adipic acid selectivities of 44%, 52%, and 4%, respectively. Notably, in the case of cyclohexane autoxidation **1** is comparable in activity to **2**, which exemplifies the halogenated porphyrin catalysts considered to be the most active hydrocarbon autoxidation catalysts known. Notably, the autoxidation of cyclohexane with **1** has a higher conversion at 2 h reaction time (8%) than with **2** at 4.7 h (5%). In addition, the higher yield (12%) of solid 98+% adipic acid collected after cooling the reactor suggests that catalyst **1** could be considered for single step production of adipic acid from cyclohexane.

Table 5
Catalytic oxidation of cyclohexane[a]

	1	2	$RuDPP_3Cl_2$
% conversion	8	5	Trace
% cyclohexanol	41	44	Trace
% cyclohexanone	47	52	Trace
% adipic acid[b]	12	4	0
Reaction time (min)	120	280	240

[a] Reactions carried out in a 300-mL stainless steel reactor at 135 °C and 80 psi O_2. 3.5×10^{-5} mol catalyst. 50 mL 1,2-dichlorobenzene, 50 mL cyclohexane.
[b] 98+% pure solid adipic acid is recovered from the cooled reactor.

4. Conclusions

In summary, **1** is an autoxidation catalyst precursor comparable in activity to the highly active halogenated iron porphyrins, exemplified by **2** in this study. The proposed mechanism suggests that the primary function of **1**, as for halogenated iron porphyrins, is to provide an active catalyst that decomposes the intermediate hydroperoxide and generates chain-propagating radicals. Although DPP catalysts are not halogenated, which enhances the stability of porphyrin catalysts, all of the C–H bonds in the DPP ligand have high bond strength ($\sim$110 kcal mol^{-1}) and are not readily abstracted compared to the reactive substrate C–H bonds. Studies of the oxygen dependence, temperature dependence, catalyst concentration dependence and maximum rates are all consistent with a radical autoxidation mechanism. In addition, the general activity of **1** as a hydrocarbon autoxidation catalyst was confirmed by its ability to catalyze cyclohexane autoxidation. The utility of catalyst **1** is enhanced by its solubility in pure hydrocarbon substrates such that no co-solvent is required to promote homogenous conditions, and low catalyst concentrations (<100 μM) can be employed to achieve near-maximum oxidation rates in neat substrates. These simple iron-phenanthroline catalyst precursors join the halogenated iron porphyrins among the most active known autoxidation catalysts, and both are much more active than cobalt naphthanate at the same temperature. The results also imply ligand dissociation as an important step in catalyst precursor activation, and the nature of the active catalyst remains under investigation.

Acknowledgments

The authors thank Arch Chemical and the University of Florida for funding.

References

[1] C. Xu, PhD dissertation, University of Florida, 1999.
[2] D.E. Richardson, C. Xu, K.A. Abboud, Catalytic oxidation of hydrocarbons, U.S. 6,258,981 (2001).
[3] J.E. Lyons, P.E. Ellis, Catal. Lett. 8 (1991) 45.
[4] T.P. Wijesekera, J.E. Lyons, P.E. Ellis, Catal. Lett. 36 (1996) 69.
[5] P.E. Ellis, J.E. Lyons, Coord. Chem. Rev. 105 (1990) 181.
[6] P.E. Ellis, J.E. Lyons, Catal. Lett. 3 (1989) 389.
[7] J.E. Lyons, P.E. Ellis, H.K. Myers, J. Catal. 155 (1995) 59.
[8] L. Reich, S.S. Stivala, Autoxidation of hydrocarbons and polyolefins, in: Kinetics and Mechanisms, Marcel Dekker, Inc., New York, 1969.
[9] P.A. MacFaul, I.W.C.E. Arends, K.U. Ingold, D.D.M. Wayner, J. Chem. Soc., Perkin Trans. 2 (2) (1997) 135.
[10] A. Bottcher, E.R. Birnbaum, M.W. Day, H.B. Gray, M.W. Grinstaff, J.A. Labinger, J. Mol. Catal., A: Chem. 117 (1997) 229.
[11] J.A. Labinger, Catal. Lett. 26 (1994) 95.
[12] M.W. Grinstaff, M.G. Hill, J.A. Labinger, H.B. Gray, Science 264 (1994) 1311.
[13] M.W. Grinstaff, M.G. Hill, E.R. Birnbaum, W.P. Schaefer, J.A. Labinger, H.B. Gray, Inorg. Chem. 34 (1995) 4896.
[14] H. Weiner, A. Trovarelli, R.G. Finke, J. Mol. Catal., A: Chem. 191 (2003) 217.
[15] R.A. Sheldon, J.K. Kochi, Oxidat. Combust. Rev. 5 (1973) 135.
[16] R.A. Sheldon, J.K. Kochi, Metal-Catalyzed Oxidations of Organic Compounds, Academic Press, New York, 1981.
[17] J.A. Howard, Homogeneous liquid phase autoxidations, in: J.K. Kochi (Ed.), Free Radicals, Wiley–Interscience, New York, 1973, pp. 3–62.
[18] R.A. Sheldon, J.K. Kochi, Adv. Catal. 25 (1976) 272.
[19] K.T. Moore, I.T. Horvath, M.J. Therien, Inorg. Chem. 39 (2000) 3125.
[20] J.P. Collin, J.P. Sauvage, Inorg. Chem. 25 (1986) 135.
[21] K.S. Hagen, Inorg. Chem. 39 (2000) 5867.
[22] J.A. Howard, K.U. Ingold, M. Symonds, Can. J. Chem. 46 (1968) 1017.
[23] B.S. Middleton, K.U. Ingold, Can. J. Chem. 45 (1967) 191.
[24] J.R. Thomas, J. Am. Chem. Soc. 89 (1967) 4872.
[25] J.A. Howard, J.E. Bennett, G. Brunton, Can. J. Chem. 59 (1981) 2253.
[26] S. Evans, J.R.L. Smith, J. Chem. Soc., Perkin Trans. 2 (2) (2000) 1541.
[27] E.R. Birnbaum, M.W. Grinstaff, J.A. Labinger, J.E. Bercaw, H.B. Gray, J. Mol. Catal., A: Chem. 104 (1995) L119.
[28] C.X. Yin, R.G. Finke, Inorg. Chem. 44 (2005) 4175.
[29] J.A. Howard, K.U. Ingold, Can. J. Chem. 46 (1968) 2655.
[30] C. Walling, J. Am. Chem. Soc. 91 (1969) 7590.
[31] D.G. Hendry, J. Am. Chem. Soc. 89 (1967) 5433.
[32] J.A. Howard, J.C. Robb, Trans. Faraday. Soc. 59 (1963) 1590.